

See discussions, stats, and author profiles for this publication at: <https://www.researchgate.net/publication/263945866>

Versatile Electronic and Magnetic Properties of Corrugated V₂O₅ Two-Dimensional Crystal and Its Derived One-Dimensional Nanoribbons: A Computational Exploration

ARTICLE *in* THE JOURNAL OF PHYSICAL CHEMISTRY C · JUNE 2011

Impact Factor: 4.77 · DOI: 10.1021/jp204174p

CITATIONS

17

READS

42

4 AUTHORS, INCLUDING:



[Qing Tang](#)

University of California, Riverside

40 PUBLICATIONS 745 CITATIONS

[SEE PROFILE](#)



[Zhen Zhou](#)

Nankai University

212 PUBLICATIONS 6,833 CITATIONS

[SEE PROFILE](#)



[Zhongfang Chen](#)

University of Puerto Rico at Rio Piedras

220 PUBLICATIONS 7,923 CITATIONS

[SEE PROFILE](#)

Versatile Electronic and Magnetic Properties of Corrugated V₂O₅ Two-Dimensional Crystal and Its Derived One-Dimensional Nanoribbons: A Computational Exploration

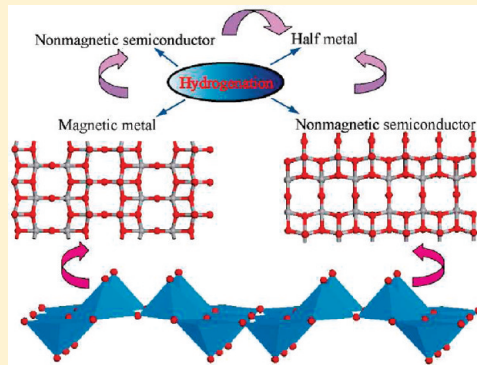
Qing Tang,^{†,‡} Fengyu Li,[‡] Zhen Zhou,^{*†} and Zhongfang Chen^{*‡}

[†]Institute of New Energy Material Chemistry, Key Laboratory of Advanced Energy Materials Chemistry (Ministry of Education), Tianjin Key Laboratory of Metal and Molecule Based Material Chemistry, Nankai University, Tianjin 300071, China

[‡]Department of Chemistry, Institute for Functional Nanomaterials, University of Puerto Rico, Rio Piedras Campus, San Juan, PR 00931

Supporting Information

ABSTRACT: Density functional theory computations were performed to investigate the structural, electronic, and magnetic properties of V₂O₅ two-dimensional (2D) crystal and its derived one-dimensional (1D) nanoribbons. The corrugated V₂O₅ 2D crystal is feasible energetically and behaves as a nonmagnetic semiconductor and can be converted into a magnetic metal by surface hydrogenation. Regardless of the ribbon width, the 1D single-layer zigzag nanoribbons are intrinsically magnetic metals, while energetically more favorable armchair analogues are nonmagnetic semiconductors. Depending on the hydrogenation sites, both zigzag and armchair V₂O₅ nanoribbons can be nonmagnetic semiconductors or magnetic half-metals.



INTRODUCTION

Graphene was once regarded as a thermodynamically unstable two-dimensional (2D) atomic crystal; however, the successful fabrication since 2004¹ has opened a new field in materials science and condensed-matter physics. Graphene exhibits exceptional optical and electronic properties significantly distinctive from its bulk form. Other changes, such as new mechanical and chemical responses, also emerge due to special geometry and high surface-to-bulk ratio.

Graphene nanoribbons (GNRs), the one-dimensional (1D) graphene, present even more intriguing properties.² Experimentally, GNRs with varying widths and edge geometries have been achieved by cutting mechanically exfoliated graphene,³ patterning epitaxially grown graphenes,⁴ unzipping carbon nanotubes,⁵ and bottom-up fabrication.⁶ The electronic and magnetic properties of NRs and their functionalized derivatives have been studied extensively, and many unusual properties have been found.^{7–16}

Similarly, inorganic 2D crystals and their derived 1D nanoribbons have unique properties closely associated with the low-dimensional quantum confinement effect and peculiar edge effect, and are promising for many applications, such as in nanocatalysis, nanoelectronic, and spintronic devices. Recently, great progress has been made on graphene and its inorganic analogues such as BN, MoS₂, NbSe₂, and Bi₂Sr₂CaCu₂O_x; these novel materials are bringing us new breakthroughs to explore other inorganic alternatives.

As a layered transition metal compound, vanadium pentoxide (V₂O₅)¹⁹ has wide applications in catalysts,²⁰ chemical sensors,²¹

optical switches,²² electrochromic devices,²³ and lithium-ion batteries.²⁴ Promoted by the technological advancements, various low-dimensional V₂O₅ nanomaterials, such as nanotubes,²⁵ nanowires, nanofibers,²⁶ nanorods,²⁷ nanobelts, and nanorolls,²⁸ have been fabricated by a variety of experimental routes, including hydrothermal synthesis,²⁹ sol–gel process,³⁰ and electrochemical deposition.³¹

Bulk V₂O₅ forms layered crystals with strong in-plane covalent bonding and weak van der Waals (vdW) coupling between layers.³² Among the three low-index surfaces, namely, the coordinately saturated (010), and the coordinately unsaturated (001) or (100), the most stable (010) surface has been the focus of theoretical investigations,³³ and can be easily produced by cleaving the weak interlayer vdW bonds and has been experimentally observed.³⁴

Unlike the hexagonal planar structure of graphene, the (010) V₂O₅ monolayer is strongly corrugated and built up of the distorted VO₅ square pyramids that share corners and edges.³⁵ Three structurally inequivalent O atoms exist on the ideal (010) monolayer (Figures 1a and 2a): the outermost single-coordinated O atoms (O1) are doubly bonded directly to the V atoms, while the other two types are two- and three-coordinated bridging O atoms (O2 and O3) located near the plane of the surface vanadium atoms, respectively.

Received: May 5, 2011

Published: June 01, 2011

This unique geometry endows the monolayer V_2O_5 with exposed (010) surface fascinating properties such as superior

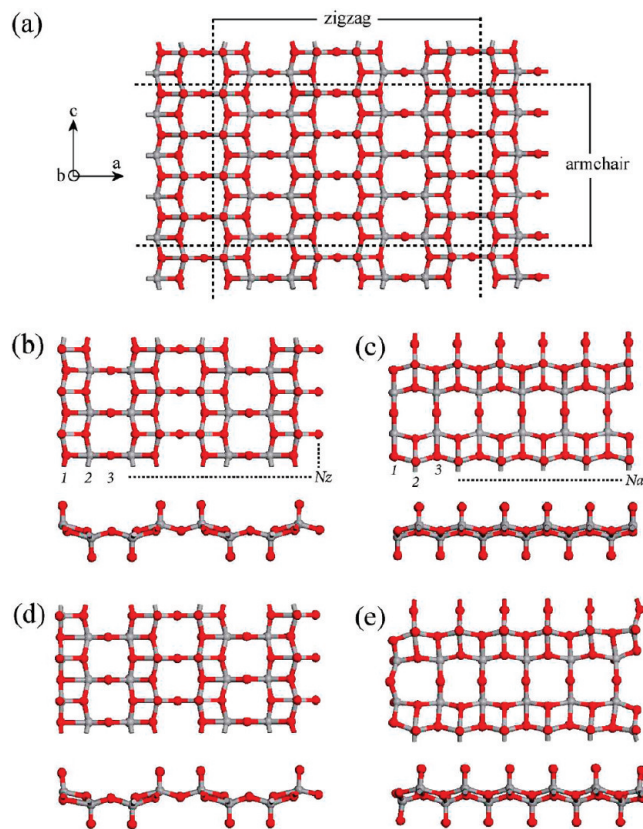


Figure 1. Geometries of the 2D single-layer V_2O_5 (top view) (a), top and side views for 1D zigzag ($N_z = 12$, containing 3 unit cells) (b) and armchair ($N_a = 12$, containing one unit cell) (c) V_2O_5 ribbons cut along zigzag or armchair lines, and the fully relaxed structures corresponding to 12-zigzag (d) and 12-armchair (e) V_2O_5 ribbons. The gray and red atoms represent V and O atoms, respectively.

catalytic ability. For example, Du et al.³⁶ pointed out that the V_2O_5 monolayer could promote the dehydrating kinetics in magnesium hydride.

Additionally, V_2O_5 nanoribbons have also been studied in experiments for many years due to their interesting properties and novel applications such as in lithium ion batteries and sensor materials.³⁷

Gaining a detailed knowledge into the properties of V_2O_5 at the atomic scale is paramount to exploit the full technological potential of V_2O_5 nanostructures. So far, single-layer V_2O_5 sheet has not been experimentally realized; a systematic theoretical investigation on its structure and properties can not only enhance our understanding to their intrinsic characteristics but also facilitate their applications. Many important questions are pending: How do the electronic and magnetic properties of the V_2O_5 nanoribbons differ from its pristine sheet? How can chemical modifications such as hydrogenation modulate the electronic properties of V_2O_5 nanosheet and nanoribbons? In this work, we aim to tackle these questions by performing density functional theory (DFT) computations.

COMPUTATIONAL METHODS

The V_2O_5 nanoribbons were constructed from the 2D single layer slab with the cleavage plane along the (010) direction (referred as the b -axis direction in the bulk phase). As in graphene and other inorganic nanoribbons, depending on the cutting direction, two types of V_2O_5 1D nanoribbons can be obtained: zigzag-like ribbons cut along c direction, forming zigzag edge on one side and an unsaturated O-bridging chain on the other side; armchair-like ribbons cut along a direction, terminated with armchair edges on both sides of the ribbon. The ribbon width is represented by the number of zigzag chains plus the O-bridging chains (N_{z+o}) or the number of armchair dimers (N_a) across the width direction. As an example, Figure 1 illustrates the top and side views of 2D single-layer V_2O_5 and its derived 1D 12-zigzag (12-armchair) ribbons.

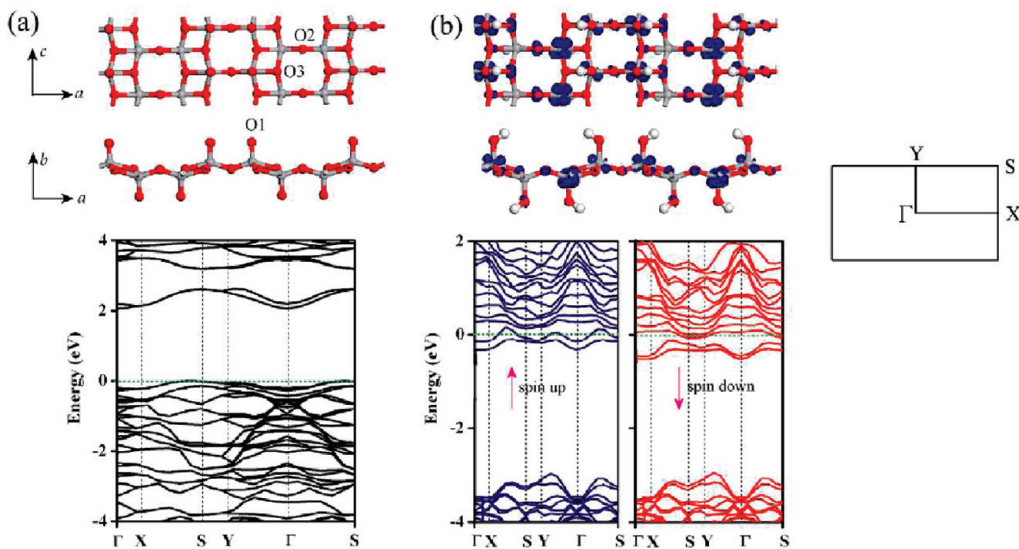


Figure 2. Optimized geometry structure (top and side view) and band structure for single layer V_2O_5 (a). The spin density distribution (top and side view) and band structure of hydrogenated V_2O_5 sheet (b). The Fermi level is denoted by a green dashed line. H atoms are represented by white balls. The 2D Brillouin zone is depicted at the right panel.

Periodic DFT computations were performed by using the plane-wave technique implemented in the Vienna *ab initio* simulation package (VASP).³⁸ Periodic boundary condition was applied along the growth direction of the V₂O₅ nanosheet/ribbons, and the supercell was large enough to ensure a vacuum spacing greater than 10 Å.

The exchange-correlation energy is described by the functional of Perdew, Burke, and Ernzerhof (PBE)³⁹ based on generalized gradient approximation (GGA) for both spin-polarized and spin-unpolarized cases. The ion-electron interaction is described with the projector augmented wave (PAW)⁴⁰ method. Pseudopotentials with 3p⁶3d⁴s¹ and 2s²2p⁴ valence electron configurations were used for V and O atoms, respectively. A 600 eV cutoff for the plane-wave basis set was used in all computations (for justification, see Table 1 in Supporting Information). The convergence threshold for optimization was set to be 10⁻⁴ eV in energy and 10⁻³ eV/Å in force. For geometry optimization, the k-point grids of 4 × 8 × 8, 4 × 8 × 1, and 1 × 1 × 5 were used for 3D bulk, 2D single sheet, and 1D ribbons, respectively, while larger k-point grids (12 × 24 × 1 and 21 k points for V₂O₅ nanosheet and nanoribbons, respectively) were used for band structure computations.

Note that the standard PBE functional cannot describe the vdW interaction between individual layers. Thus, we adopted the recently developed PBE-D2 method⁴¹ with the inclusion of dispersion energy correction. PBE-D2 has been proven effective in treating V₂O₅ layered materials, as demonstrated by Bučko et al.⁴² and us (see the Supporting Information for our test computations). In this work both the single-layer sheet and ribbons were computed based on PBE functional, while the results of bulk V₂O₅ and 2-layer (3-layer) zigzag ribbons were based on the PBE-D2 method.

To evaluate the stability of V₂O₅ nanoribbons, the binding energy per atom (E_b) is computed by using the following definition: $E_b = (nE_V + mE_O - E_{V_nO_m})/(n + m)$, where E_V , E_O , and $E_{V_nO_m}$ represent the total energies of free V atom, O atom, and V₂O₅ NRs per supercell, respectively. n (m) is the number of V (O) atoms in a supercell. According to this definition, systems with larger E_b values are energetically more favorable.

RESULTS AND DISCUSSION

Pristine 2D Single-Layer V₂O₅. We first modeled the 2D single-layer V₂O₅ by a periodic slab (Figure 2a). The single layer is composed of six planar atom layers (four for O atoms and two for V atoms), where every V or O atom is coordinately saturated. After structural relaxation, the atomic positions changed only slightly compared with those in the bulk phase. The vanadyl O1 atoms stick out of the surface in parallel rows along b direction and are doubly bonded to V atoms with a distance of 1.60 Å. The bridging O2 atoms are connected to two V atoms along a direction with the equal V–O bond lengths of 1.79 Å, while the bridging O3 atoms coordinated to three V atoms have two shorter (1.89 Å) V–O bonds and one longer (2.03 Å) V–O bond along the c and a direction, respectively.

The electronic structure of the single layer sheet also resembles that of the bulk very closely. Both the single-layer and bulk V₂O₅ are nonmagnetic semiconductors, though the monolayer has a slightly larger indirect gap (1.94 eV, Figure 2a) than the bulk (1.91 eV, see Figure S2). Moreover, the binding energies of single-layer and bulk V₂O₅ are also very similar (7.48 and 7.54 eV/atom, respectively).

In short, the single layer (010) slab has very similar structural and electronic properties and stability to its bulk crystal, matching well with previous theoretical prediction.³³

Hydrogenated 2D Single-Layer V₂O₅. The outmost surface O1 atoms are prone to hydrogenation. When saturated by H atoms, the resulting surface is assembled by alternate –OH groups. Consequently, the V–O1 bond distance is elongated to 1.79 Å, compared with the V–O1 double bond length of 1.60 Å in the pristine sheet.

Astonishingly, total energy computation indicates that the hydrogenated sheet has a magnetic ground state with a total magnetic moment of ~4.0 μ_B per unit cell. The spin-polarized state is energetically more preferable than the spin-nonpolarized state by ~0.37 eV per unit cell.

The magnetic moment mainly comes from the 3d orbitals of V atoms and 2p orbitals of bridging O2 or O3 atoms (see the spin density contribution in Figure 2b). The magnetism contributed from surface O1 atoms is extremely weak.

The electronic structure also differs strongly from the pristine sheet (Figure 2b): the single-layer sheet is of semiconducting character, while its hydrogenated derivative is metallic. Both the spin-up and spin-down channels are strongly metalized near the Fermi level. The partial density of states (PDOS) indicates that the states crossing the Fermi level arise mainly from the V 3d orbital and O 2p orbital (Figure S3).

Thus, surface hydrogenation offers an important way to modulating the electronic and magnetic properties of single-layer V₂O₅ sheet.

Pristine 1D Single-Layer V₂O₅ Nanoribbons. Two types of nanoribbons with either zigzag-terminated or armchair-terminated edge (Figure 1) can be obtained depending on different cutting directions. The fully relaxed 12-zigzag and 12-armchair V₂O₅ NRs (Figure 1d,e) have the widths of 21.3 and 19.5 Å, respectively. The edge atoms in both ribbons are strongly distorted.

Specifically, for 12-zigzag NR, the edge V–O zigzag chain on the left side of the ribbon is optimized to a nearly linear chain, where the edge O atoms (V atoms) shift outward (inward) from the corrugated V–O plane. As a consequence, the bond distance of edge V to subedge O is contracted to 1.88 Å, while the distance between edge O and subedge V is elongated to 2.34 Å, compared with the original V–O bond length of 2.03 Å in the 2D monolayer slab. On the other hand, the edge bridging O chain on the right side of the ribbon shifts inward and leads to the contraction of edge O–V bond (reduced from 1.79 Å in monolayer sheet to 1.67 Å), accompanied by the expansion of terminal O1–V bond (to 1.64 Å) located at the subedge site. The edge V–O bond length within the same zigzag chain (left side) is uniformly 1.88 Å.

For 12-armchair NR, the edge reconstruction becomes more significant. Specifically, the edge O (V) atoms drastically move outward (inward) across the width direction, yielding two non-linear edge armchair chains. Consequently, the distance between edge O (V) and subedge V (O) bond length is elongated to 1.85 Å (shortend to 1.78 Å). The edge O2 or O3 atoms in a same armchair chain have two distinct O–V distances (1.83 and 1.81 Å). The terminal O1–V (edge V site) bond deviates slightly from the normal direction, and the edge O1–V bond distance (1.61 Å) is a little longer than the inner one (1.60 Å).

To determine the magnetic ground state, we performed both spin-polarized and spin-nonpolarized total energy computations for a series of zigzag and armchair V₂O₅ NRs. Regardless of the

Table 1. Energy Difference (ΔE) between Spin-Polarized State and Spin-Nonpolarized State and the Total Magnetic Moment (M) per Unit Cell for a Series of Zigzag V_2O_5 Nanoribbons with Different Width N_{z+o} ^a

	N_{z+o}					
	6	12	18	24	30	36
ΔE (eV)	-0.078	-0.188	-0.209	-0.226	-0.237	-0.247
M (μ_B)	0.83 (0.415)	1.15 (0.288)	1.45 (0.242)	1.25 (0.156)	1.23 (0.123)	1.22 (0.102)

^a The numbers in the parentheses are the unit magnetic moment per V_2O_5 formula.

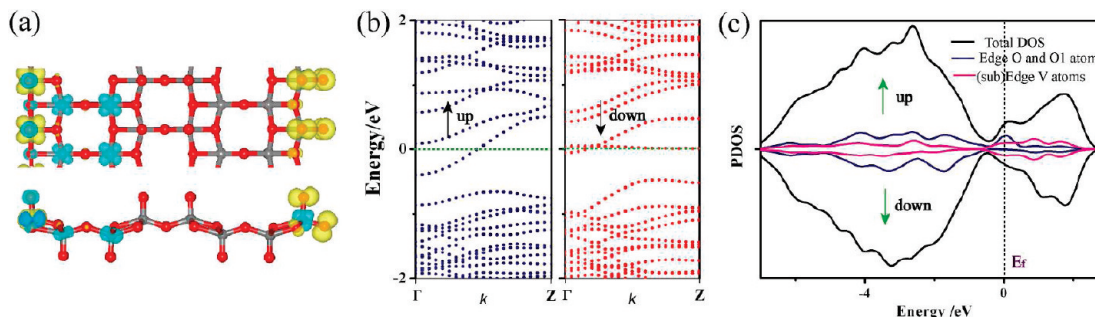


Figure 3. Top and side view of the spatial spin density distribution for 12-zigzag V_2O_5 nanoribbons (a), band structure (b), and partial density of states (c) for 12-zigzag V_2O_5 nanoribbons.

ribbon widths, the ground states of zigzag NRs are ferromagnetic (for $N_{z+o} = 6-36$); by contrast, the armchair NRs are nonmagnetic (for $N_a = 6-20$).

Table 1 summarizes the energy difference (ΔE) between the spin-polarized and spin-nonpolarized state and the total magnetic moment per unit cell for zigzag ribbons with N_{z+o} ranging from 6 to 36. Clearly, ΔE increases with increasing the ribbon width; thus, the ferromagnetic state is expected to be rather stable in wider ribbons. The total magnetic moment (M) increases initially until $N_z = 18$ and then decreases as a function of the width. Naturally, the average magnetic moment per V_2O_5 unit decreases continuously with increasing ribbon width but remains sizable for all the NRs considered in this study.

This phenomenon can be explained by the spatial spin density distribution (Figure 3a). In the case of 12-zigzag NR, the induced ferromagnetism arises mainly from the 2p orbitals of the edge O atoms (unsaturated bridging O₂, O₃ and saturated terminal O₁ atoms) and the 3d orbitals of the edge and subedge V atoms, while the inner V atoms only contribute slightly. As the ribbon width increases, the ratio of the edge O atoms vs the total atoms decreases, resulting in weaker magnetism in wider ribbons. The magnetism should vanish as the ribbon is infinitely wide and ultimately approximate the nonmagnetic behaviors as in the 2D single layer sheet.

Cutting the semiconducting 2D V_2O_5 single sheet into 1D NRs leads to dramatic change of the electronic structure for zigzag NRs: all the zigzag V_2O_5 NRs considered here ($N_{z+o} = 6-36$) are ferromagnetically metallic with considerable bands crossing the Fermi level in both minority and majority spin channels. For example, the spin-resolved band structure of 12-zigzag V_2O_5 NR (Figure 3b) displays a typical metallic behavior, and the bands crossing the Fermi level are predominated by the edge O and O₁ atoms (2p states) as well as the edge and subedge V atoms (3d states) (Figure 3c).

In stark contrast to the metallic characteristic in zigzag V_2O_5 NRs, all the armchair NRs are semiconducting. Take 12-armchair

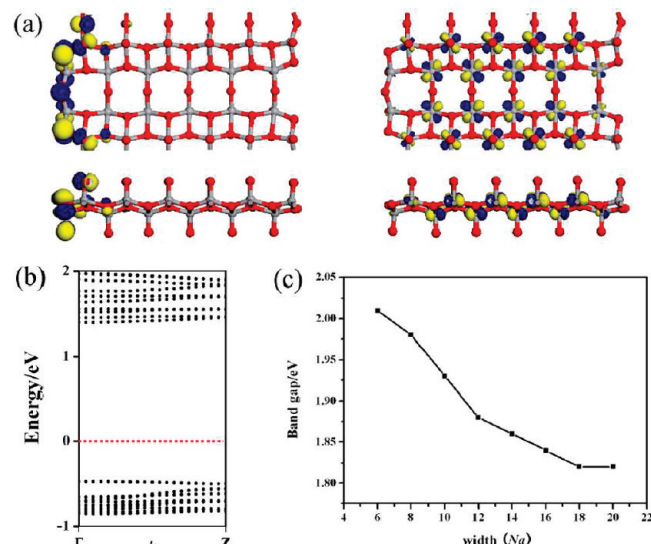


Figure 4. Partial charge density of the top valence band (left) and bottom conduction band (right) at Γ point for 12-armchair V_2O_5 NR (a, top and side view), the band structure of 12-armchair V_2O_5 NR (b), and the band gap variation as a function of ribbon width N_a (c).

V_2O_5 NR as an example; both valence band and conduction band close to Γ direction are rather flat, leading to a direct energy gap of 1.88 eV at the Γ point (Figure 4b). The partial charge density analysis reveals that the highest occupied state (Figure 4a, left) primarily consists of the 2p orbitals of edge bridging O₂ (O₃) and terminal O₁ atoms along with the subedge O₁ atoms, while the lowest empty state (Figure 4a, right) mostly comes from the 3d orbitals of inner V atoms and distributes uniformly within the ribbon system.

The band gap of armchair V_2O_5 NRs gradually decreases with increasing the ribbon width (Figure 4c) and converges to almost

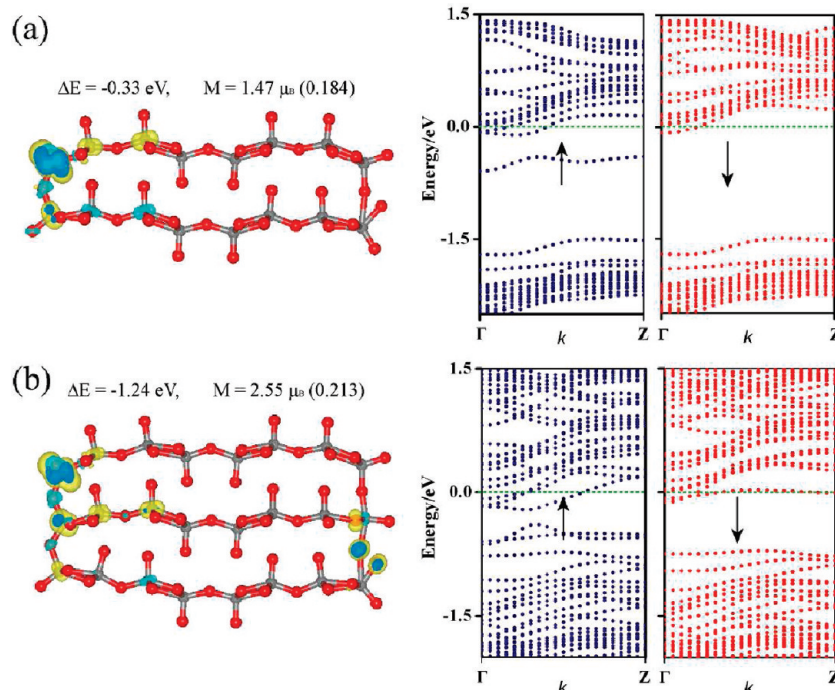


Figure 5. Optimized 12-zigzag V₂O₅ nanoribbons with two layers (a) and three layers (b), respectively. The left part shows the energy difference ΔE between spin-polarized and spin-nonpolarized state, total magnetic moment M (unit magnetic moment per V₂O₅ formula, indicated in parentheses) and spatial spin density distribution. The right part presents the corresponding band structures.

a constant value of 1.82 eV when the ribbon exceeds a certain critical width ($N_a = 18$). This is mainly attributed to the quantum confinement effect.

Pristine 1D Multilayer Zigzag V₂O₅ Nanoribbons. The unusual magnetic and electronic properties of single-layer zigzag V₂O₅ NRs inspired us to further investigate zigzag NRs up to three stacking layers to examine the thickness effect.

These multilayer NRs were cleaved directly from the bulk V₂O₅, and the width was set to be 21.3 Å (i.e., 12-zigzag NRs). After relaxation, interlayer bonds formed for both two- and three-layer 12-zigzag NRs (Figure 5a,b): at the outermost zigzag chains, the inward-pointed edge terminal O1 atoms are bonded to the closest V atoms in the adjacent layer, whereas the inner part of the ribbon remains separated.

Similar edge bond formation also occurs in multilayer ZnO zigzag NRs;⁴³ however, their magnetic behaviors drastically differ from the V₂O₅ analogues. For ZnO zigzag NRs, the single-layer magnetism arises from the unpaired spins of edge oxygen atoms, while the magnetism completely disappears in even-numbered layers after the edge O–Zn bonds form. In contrast, the ferromagnetic behaviors observed in single-layer V₂O₅ zigzag NRs are well preserved in two- and three-layered V₂O₅ NRs. Both the energy difference between the spin-polarized and spin-unpolarized state (ΔE) and total magnetic moment (M) increases as the number of layers increases. The total magnetic moment of 12-zigzag system corresponding to two and three layers is 1.47 and 2.55 μ_B , respectively. Yet the unit magnetic moment per V₂O₅ formula (0.184 and 0.213 μ_B) is much smaller than that of the single-layer case (0.288 μ_B). Both the V 3d orbitals and O 2p orbitals (mainly the edge sites) contribute to magnetism (see the spin density distribution in Figure 5a,b, left), which is not completely compensated even when the edge V–O bonds form.

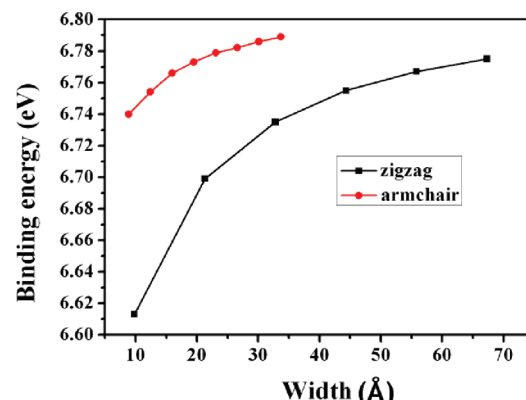


Figure 6. Binding energy per atom for zigzag ($6 \leq N_z \leq 36$) and armchair ($6 \leq N_z \leq 20$) V₂O₅ nanoribbons as a function of ribbon width.

The two-layer and three-layer 12-zigzag NRs inherit the metallic feature of the single-layer ribbons, as indicated by the computed electronic band structures (Figure 5). The total magnetic moment M changes less in wider zigzag ribbons (Table 1). For a specific zigzag NR with the given width, the total magnetic moment increases with increasing thickness. As long as the width and thickness of the zigzag ribbons are at the nanoscale, the predicted magnetic and metallic behaviors are expected to be well reserved regardless of ribbon width or thickness.

Thermodynamic Stability of V₂O₅ NRs. We evaluated the thermodynamic stability of V₂O₅ NRs to examine the feasibility to experimentally realize the predicted systems. For both zigzag and armchair V₂O₅ NRs, the binding energy increases

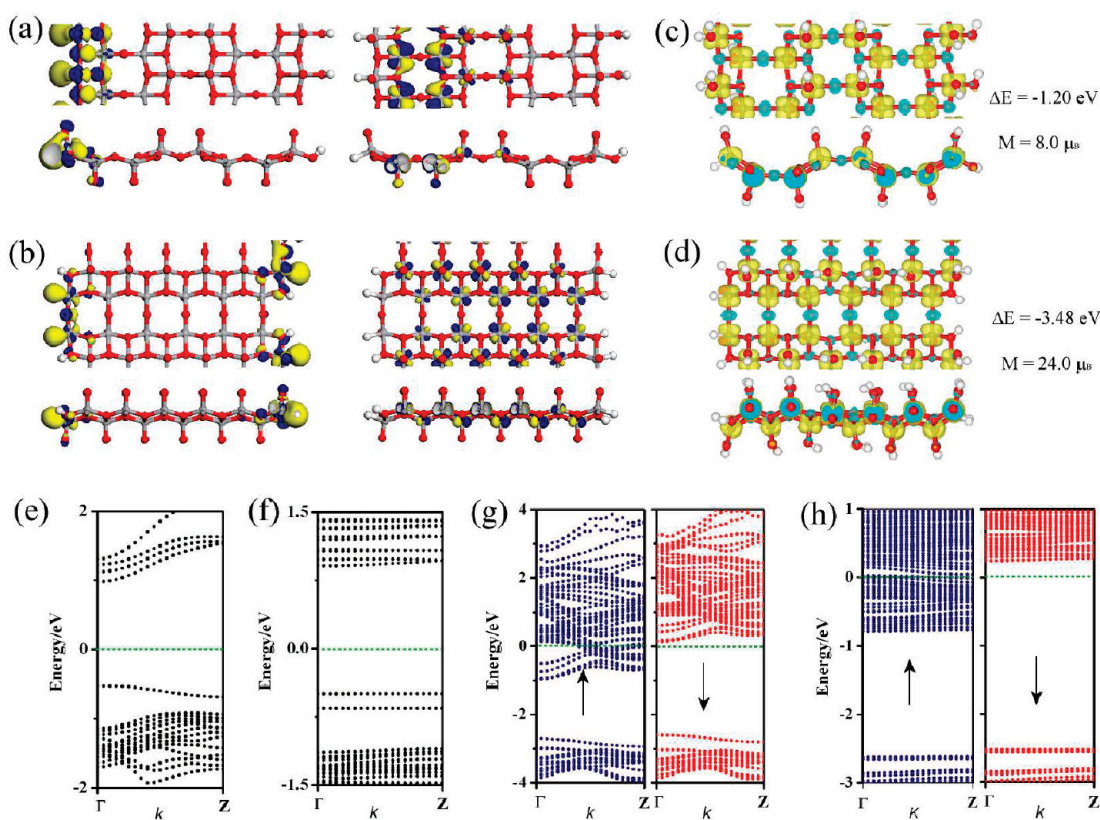


Figure 7. Partial charge density of VBM (left) and CBM (right) at the Γ point for 12-zigzag (a) and 12-armchair (b) NRs where only the edge atoms are saturated by H atoms, and their corresponding band structures are displayed in (e) and (f), respectively. Spatial spin density distribution of 12-zigzag (c) and 12-armchair (d) NRs where both the surface and edge atoms are saturated by H atoms, with their corresponding band structures in (g) and (h), respectively.

monotonically as the ribbon width increases (Figure 6). Thus, the wider the ribbon is, the more stable the structure becomes (higher E_b). Moreover, the binding energies of armchair NRs are much larger than those of zigzag ones for comparable widths and of higher thermodynamic stability.

Hydrogenated Pristine 1D Single-Layer V_2O_5 Nanoribbons. Since the zigzag or armchair-terminated edge atoms are coordinately unsaturated and the surface atoms are sensitive to H adsorption, it is necessary to explore how the electronic and magnetic properties of V_2O_5 NRs rely on edge and surface hydrogenation. Here 12-zigzag and 12-armchair V_2O_5 NRs were chosen as two representative models to investigate the hydrogenation effect.

First we considered the edge hydrogenation. As evidently described in Figure 7a,b, both 12-zigzag and 12-armchair NRs become less distorted after all the edge dangling bonds are saturated by H atoms.

Edge hydrogenation converts the original ferromagnetic and metallic 12-zigzag NR to be nonmagnetic and semiconducting (with a direct band gap of 1.48 eV at Γ point, Figure 7c), while the edge-hydrogenated 12-armchair NR retains the nonmagnetic and semiconducting characteristic of the original armchair V_2O_5 NR, though the band gap is narrowed (from 1.88 to 1.40 eV) by edge hydrogenation (Figure 7d). Thus, the introduction of H atoms at the edges drastically altered the electronic properties of V_2O_5 NRs, especially for zigzag ones.

The partial charge density distributions of both edge-hydrogenated 12-zigzag and 12-armchair NRs (Figure 7a,b) are very

similar. In these two cases, the valence band maximum (VBM) is largely composed of the edge H atoms (1s orbital) and edge O atoms (2p orbital), while the conduction band minimum (CBM) is distributed onto the inner V atoms (3d orbital).

Second, we investigated the fully hydrogenated 12-zigzag and 12-armchair V_2O_5 NRs (at both edge atoms and surface O1 atoms). The hydrogenated surfaces become slightly deviated from the normal orientations due to the newly formed O–H bonds (Figure 7c,d).

Such a full hydrogenation transforms the original nonmagnetic 12-armchair NR into ferromagnetic, while the 12-zigzag retains ferromagnetic. Compared with the non-hydrogenated case, the energy difference between spin-polarized and spin-unpolarized states (ΔE) and total magnetic moment per unit cell (M) drastically increase (Figure 7). Overall, both 12-zigzag and 12-armchair NRs share similar spin density distributions (Figure 7c,d), which suggests that such strong magnetism is mostly ascribed to the V atoms (3d orbital) and uniformly distributed into the whole system, with some weak contribution from O atoms (2p orbital).

In addition, the fully hydrogenated 12-zigzag and 12-armchair V_2O_5 NRs also share remarkable similarities in electronic structures. Remarkably, the full hydrogenation converts both 12-zigzag and 12-armchair V_2O_5 NRs into half metals (Figure 7g,h). In these two ribbons, the spin-up channels are metallic, while the spin-down channels are semiconducting with a direct band gap of 2.66 eV for 12-zigzag NR and 2.73 eV for 12-armchair NR at the Γ point. This indicates a clear half-metallic character and qualifies the fully hydrogenated V_2O_5 NRs as good candidates for spintronics applications.

On the basis of the above discussion, we come to recognize that hydrogenation plays an important role in modulating the electronic and magnetic properties of single-layer V_2O_5 NRs. For zigzag NRs, a magnetic metal \rightarrow nonmagnetic semiconductor \rightarrow magnetic half-metal transition occurs depending on the hydrogenation sites. While for armchair NRs, variation of hydrogenation sites is also accompanied by a nonmagnetic semiconductor \rightarrow magnetic half-metal transition.

CONCLUSION

In this work, we presented detailed DFT investigations on the geometric and electronic structures and magnetic properties of V_2O_5 2D crystal and its derived nanoribbons with zigzag or armchair-shaped edges.

The pristine 2D monolayer V_2O_5 is of feasible stability and acts as a nonmagnetic semiconductor but resorts to a ferromagnetic metal after surface hydrogenation.

When cutting into 1D nanoribbons, novel properties emerge: zigzag V_2O_5 nanoribbons possess ferromagnetic and metallic behaviors without the introduction of metal impurities, irrespective of ribbon width or thickness; armchair nanoribbons, however, are nonmagnetic and semiconducting. Binding energy computations clearly identify that armchair V_2O_5 nanoribbons are energetically more favorable than zigzag nanoribbons.

Hydrogenation offers an effective approach for engineering the electronic and magnetic properties of V_2O_5 NRs. Both zigzag and armchair NRs are all nonmagnetic semiconductors when only the edge atoms are hydrogenated and are further transformed into half-metals after the surface and edge atoms are totally hydrogenated.

The fast-growing success in isolating various 2D monolayer crystals makes us highly optimistic that monolayer V_2O_5 and 1D nanoribbons can be realized experimentally in the near future. As one of the most important functional oxides, V_2O_5 displays diverse properties and receives active attention that it deserves. Hopefully, the theoretical insights presented in our work will prompt further efforts in the experimental synthesis and characterization of V_2O_5 nanosheets/ribbons and their applications in nanoelectronics, spintronics, and other fields.

ASSOCIATED CONTENT

S Supporting Information. Cut-off energy testing results and comparison between PBE and PBE-D2 method based on bulk V_2O_5 ; band structures of bulk V_2O_5 and two-layer or three-layer sheets as well as partial density of states of surface-hydrogenated single-layer V_2O_5 . This material is available free of charge via the Internet at <http://pubs.acs.org>.

AUTHOR INFORMATION

Corresponding Author

*E-mail: zhouchen@nankai.edu.cn (Z.Z.), zhongfangchen@gmail.com (Z.C.).

ACKNOWLEDGMENT

Support in China by NSFC (21073096), Fundamental Research Funds for the Central Universities, MOE NCET (08-0293) and Innovation Research Team (IRT0927), and in USA by NSF Grant EPS-1010094 and the NASA IDEAS grant of University of Puerto Rico, is gratefully acknowledged. This

research was also supported in part by the National Science Foundation through TeraGrid resources.

REFERENCES

- (1) (a) Novoselov, K. S.; Geim, A. K.; Morozov, S. V.; Jiang, D.; Zhang, Y.; Dubonos, S. V.; Grigorieva, I. V.; Firsov, A. A. Electric Field Effect in Atomically Thin Carbon Films. *Science* **2004**, *306*, 666. (b) Geim, A. K.; Novoselov, K. S. The Rise of Graphene. *Nature Mater.* **2007**, *6*, 183–191.
- (2) For recent reviews, see: (a) Castro Neto, A. H.; Guinea, F.; Peres, N. M. R.; Novoselov, K. S.; Geim, A. K. The Electronic Properties of Graphene. *Rev. Mod. Phys.* **2009**, *81*, 109–162. (b) Dutta, S.; Pati, S. K. Novel Properties of Graphene Nanoribbons: a Review. *J. Mater. Chem.* **2010**, *20*, 8207–8223. (c) Terrones, M.; Botello-Méndez, A. R.; Campos-Delgado, J.; López-Urías, F.; Vega-Cantí, Y. I.; Rodríguez-Macías, F. J.; Elías, A. L.; Muñoz-Sandoval, E.; Cano-Márquez, A. G.; Charlier, J.-C.; Terrones, H. Graphene and Graphite Nanoribbons: Morphology, Properties, Synthesis, Defects and Applications. *Nano Today* **2010**, *5*, 351–372.
- (3) (a) Li, X.; Wang, X.; Zhang, L.; Lee, S.; Dai, H. Chemically Derived, Ultrasmooth Graphene Nanoribbon Semiconductors. *Science* **2008**, *319*, 1229–1232. (b) Zhang, Y.; Tan, Y.; Stormer, H. L.; Kim, P. Experimental Observation of the Quantum Hall Effect and Berry's Phase in Graphene. *Nature* **2005**, *438*, 201–204.
- (4) Berger, C.; Song, Z.; Li, X.; Wu, X.; Brown, N.; Naud, C.; Mayou, D.; Li, T.; Hass, J.; Marchenkov, A. N.; Conrad, E. H.; First, P. N.; de Heer, W. A. Electronic Confinement and Coherence in Patterned Epitaxial Graphene. *Science* **2006**, *312*, 1191–1196.
- (5) (a) Jiao, L.; Zhang, L.; Wang, X.; Diankov, G.; Dai, H. Narrow Graphene Nanoribbons From Carbon Nanotubes. *Nature* **2009**, *458*, 877. (b) Kosynkin, D. V.; Higginbotham, A. L.; Sinitskii, A.; Lomeda, J. R.; Dimiev, A.; Price, B. K.; Tour, J. M. Longitudinal Unzipping of Carbon Nanotubes to Form Graphene Nanoribbons. *Nature* **2009**, *458*, 872–876.
- (6) Cai, J.; Ruffieux, P.; Jaafar, R.; Bieri, M.; Braun, T.; Blankenburg, S.; Muoth, M.; Seitsonen, A. P.; Saleh, M.; Feng, X.; Müllen, K.; Fasel, M. Attractively Precise Bottom-up Fabrication of Graphene Nanoribbons. *Nature* **2010**, *466*, 470–473.
- (7) Barone, V.; Hod, O.; Scuseria, G. E. Electronic Structure and Stability of Semiconducting Graphene Nanoribbons. *Nano Lett.* **2006**, *6*, 2748–2754.
- (8) Son, Y. W.; Cohen, M. L.; Louie, S. G. Energy Gaps in Graphene Nanoribbons. *Phys. Rev. Lett.* **2006**, *97*, 216803.
- (9) Ritter, K. A.; Lyding, J. W. The Influence of Edge Structure on the Electronic Properties of Graphene Quantum Dots and Nanoribbons. *Nature Mater.* **2009**, *8*, 235–242.
- (10) Kudin, K. N. Zigzag Graphene Nanoribbons with Saturated Edges. *ACS Nano* **2008**, *2*, 516–522.
- (11) Li, Y.; Zhou, Z.; Shen, P.; Chen, Z. Structural and Electronic Properties of Graphene Nanoribbons. *J. Phys. Chem. C* **2009**, *113*, 15043–15045.
- (12) Kan, E.; Li, Z.; Yang, J.; Hou, J. G. Half-Metallicity in Edge-Modified Zigzag Graphene Nanoribbons. *J. Am. Chem. Soc.* **2008**, *130*, 4224–4225.
- (13) Wu, M.; Wu, X.; Zeng, X. C. Exploration of Half Metallicity in Edge-Modified Graphene Nanoribbons. *J. Phys. Chem. C* **2010**, *114*, 3937–3944.
- (14) Li, Y. F.; Zhou, Z.; Shen, P. W.; Chen, Z. Spin Gapless Semiconductor-Metal-Half metal Properties in Nitrogen-Doped Zigzag Graphene Nanoribbons. *ACS Nano* **2009**, *3*, 1952–1958.
- (15) Yan, Q.; Huang, B.; Yu, J.; Zheng, F.; Zang, J.; Wu, J.; Gu, B. L.; Liu, F.; Duan, W. Intrinsic Current-Voltage Characteristics of Graphene Nanoribbon Transistors and Effect of Edge Doping. *Nano Lett.* **2007**, *7*, 1469–1473.
- (16) Son, Y. W.; Cohen, M. L.; Louie, S. G. Half-metallic Graphene Nanoribbons. *Nature* **2006**, *444*, 347–349.
- (17) Novoselov, K. S.; Jiang, D.; Schedin, F.; Booth, T. J.; Khotkevich, V. V.; Morozov, S. V.; Geim, A. K. Two-dimensional Atomic Crystals. *Proc. Natl. Acad. Sci. U.S.A.* **2005**, *102*, 10451–10453.

- (18) For recent reviews and some most recent studies, see: (a) Seo, J.-W.; Jun, Y.-W.; Park, S.-W.; Nah, H.; Moon, T.; Park, B.; Kim, J.-G.; Kim, Y.-J.; Cheon, J. Two-dimensional Nanosheet Crystals. *Angew. Chem., Int. Ed.* **2007**, *46*, 8828–8831. (b) Osada, M.; Sasaki, T. Exfoliated Oxide Nanosheets: New Solution to Nanoelectronics. *J. Mater. Chem.* **2009**, *19*, 2503–2511. (c) Golberg, D.; Bando, Y.; Huang, Y.; Terao, T.; Mitome, M.; Tang, C.; Zhi, C. Boron Nitride Nanotubes and Nanosheets. *ACS Nano* **2010**, *4*, 2979. (d) Mas-Ballesté, R.; Gómez-Navarro, C.; Gómez-Herrero, J.; Zamora, F. 2D Materials: To Graphene and Beyond. *Nanoscale* **2011**, *3*, 20–30. (e) Castro Neto, A. H.; Novoselov, K. Two-Dimensional Crystals: Beyond Graphene. *Mater. Express.* **2011**, *1*, 10–17. (f) Gao, X. F.; Zhou, Z.; Zhao, Y. L.; Nagase, S.; Zhang, S. B.; Chen, Z. Comparative Study of Carbon and BN Nanographenes: Ground Electronic States and Gap Energy Engineering. *J. Phys. Chem. C* **2008**, *112*, 12677–12682. (g) Chen, W.; Li, Y. F.; Yu, G. T.; Zhou, Z.; Chen, Z. Electronic Structure and Reactivity of Boron Nitride Nanoribbons with Stone-Wales Defects. *J. Chem. Theory Comput.* **2009**, *5*, 3088–3095. (h) Chen, W.; Li, Y.; Yu, G.; Li, C.; Zhang, S. B.; Zhou, Z.; Chen, Z. Hydrogenation: A Simple Approach To Realize Semiconductor-Half-Metal-Metal Transition in Boron Nitride Nanoribbons. *J. Am. Chem. Soc.* **2010**, *132*, 1699. (i) Zeng, H.; Zhi, C.; Zhang, Z.; Wei, X.; Wang, X.; Guo, W.; Bando, Y.; Golberg, D. “White Graphenes”: Boron Nitride Nanoribbons via Boron Nitride Nanotube Unwrapping. *Nano Lett.* **2010**, *10*, 5049–5055. (j) Li, Y.; Zhou, Z.; Zhang, S.; Chen, Z. MoS₂ Nanoribbons: High Stability and Unusual Electronic and Magnetic Properties. *J. Am. Chem. Soc.* **2008**, *130*, 16739–16744. (k) Wang, Z.; Li, H.; Liu, Z.; Shi, Z.; Lu, J.; Suenaga, K.; Joung, S.; Okazaki, T.; Gu, Z.; Zhou, J.; Gao, Z.; Li, G.; Sanvito, S.; Wang, E.; Iijima, S. Mixed Low-Dimensional Nanomaterial: 2D Ultra-narrow MoS₂ Inorganic Nanoribbons Encapsulated in Quasi-1D Carbon Nanotubes. *J. Am. Chem. Soc.* **2010**, *132*, 13840–13847. (l) Tang, Q.; Li, Y.; Zhou, Z.; Chen, Y.; Chen, Z. Tuning Electronic and Magnetic Properties of Wurtzite ZnO Nanosheets by Surface Hydrogenation. *ACS Appl. Mater. Interfaces* **2010**, *2*, 2442–2447. (m) Tang, Q.; Cui, Y.; Li, Y. F.; Zhou, Z.; Chen, Z. How Do Surface and Edge Effects Alter the Electronic Properties of GaN Nanoribbons? *J. Phys. Chem. C* **2011**, *115*, 1724–1731. (n) Sun, L.; Li, Y.; Li, Z.; Li, Q.; Zhou, Z.; Chen, Z.; Yang, J.; Hou, J. G. Electronic Structures of SiC Nanoribbons. *J. Chem. Phys.* **2008**, *129*, 174114. (o) Li, Y. F.; Li, F. Y.; Zhou, Z.; Chen, Z. SiC₂ Silagraphene and Its One-Dimensional Derivatives: Where Planar Tetracoordinate Silicon Happens. *J. Am. Chem. Soc.* **2011**, *133*, 900–908.
- (19) Schoiswohl, J.; Surnev, S.; Netzer, F. P.; Kresse, G. Vanadium Oxide Nanostructures: From Zero- to Three-dimensional. *J. Phys.: Condens. Matter* **2006**, *18*, R1–R14.
- (20) Ponzi, M.; Duschatzky, C.; Carrascull, A.; Ponzi, E. Obtaining Benzaldehyde via Promoted V₂O₅ Catalysts. *Appl. Catal., A* **1998**, *169*, 373–379.
- (21) (a) Micocci, G.; Serra, A.; Tepore, A.; Capone, S.; Rella, R.; Siciliano, P. Properties of Vanadium Oxide Thin Films for Ethanol Sensor. *J. Vac. Sci. Technol. A* **1997**, *15*, 34–38. (b) Livage, J. Vanadium Pentoxide Gels. *Chem. Mater.* **1991**, *3*, 578–593.
- (22) Chain, E. E. Optical Properties of Vanadium Dioxide and Vanadium Pentoxide Thin Films. *Appl. Opt.* **1991**, *30*, 2782–2787.
- (23) Cheng, K.; Chen, F.; Kai, J. V₂O₅ Nanowires as a Functional Material For Electrochromic Device. *Sol. Energy Mater. Sol. Cells* **2006**, *90*, 1156–1165.
- (24) (a) Poizot, P.; Laruelle, S.; Gruegeon, S.; Dupont, L.; Tarascon, J. M. Nano-sized Transition-metal Oxides as Negative-electrode Materials for Lithium-ion Batteries. *Nature* **2000**, *407*, 496–499. (b) Cao, A.; Hu, J.; Liang, H.; Wan, L. Self-Assembled Vanadium Pentoxide (V₂O₅) Hollow Microspheres from Nanorods and Their Application in Lithium-Ion Batteries. *Angew. Chem., Int. Ed.* **2005**, *44*, 4391–4395. (c) Wu, C.; Xie, Y. Promising Vanadium Oxide and Hydroxide Nanostructures: From Energy Storage to Energy Saving. *Energy Environ. Sci.* **2010**, *3*, 1191–1206.
- (25) Muhr, H. J.; Krumeich, F.; Schönholzer, U. P.; Bieri, F.; Niederberger, M.; Gauckler, L. J.; Nesper, R. Vanadium Oxide Nanotubes—A New Flexible Vanadate Nanophase. *Adv. Mater.* **2000**, *12*, 231–234.
- (26) Gu, G.; Schmid, M.; Chiu, P.; Minett, A.; Fraysse, J.; Kim, G.; Roth, S.; Kozlov, M.; Muñoz, E.; Baughman, R. H. V₂O₅ Nanofibre Sheet Actuators. *Nature Mater.* **2003**, *2*, 316–319.
- (27) Pinna, N.; Wild, U.; Urban, J.; Schlögl, R. Divanadium Pentoxide Nanorods. *Adv. Mater.* **2003**, *15*, 329–331.
- (28) Li, B.; Xu, Y.; Rong, G.; Jing, M.; Xie, Y. Vanadium Pentoxide Nanobelts and Nanorolls: From Controllable Synthesis to Investigation of Their Electrochemical Properties and Photocatalytic Activities. *Nanotechnology* **2006**, *17*, 2560–2566.
- (29) Chirayil, T.; Zavalij, P. Y.; Whittingham, M. S. Hydrothermal Synthesis of Vanadium Oxides. *Chem. Mater.* **1998**, *10*, 2629–2640.
- (30) Özer, N. Electrochemical Properties of Sol-gel Deposited Vanadium Pentoxide Films. *Thin Solid Films* **1997**, *305*, 80–87.
- (31) Takahashi, K.; Limmer, S. J.; Wang, Y.; Cao, G. Synthesis and Electrochemical Properties of Single-Crystal V₂O₅ Nanorod Arrays by Template-Based Electrodeposition. *J. Phys. Chem. B* **2004**, *108*, 9795–9800.
- (32) Londero, E.; Schröder, E. Role of Van der Waals Bonding in the Layered Oxide V₂O₅: First-principles Density-functional Calculations. *Phys. Rev. B* **2010**, *82*, 054116.
- (33) (a) Michalak, A.; Witko, M.; Hermann, K. Density Functional Cluster Studies on the (010) Surface of Vanadium Pentoxide. *Surf. Sci.* **1997**, *375*, 385–394. (b) Chakrabarti, A.; Hermann, K.; Družinic, R.; Witko, M.; Wagner, F.; Petersen, M. Geometric and Electronic Structure of Vanadium Pentoxide: A Density Functional Bulk and Surface Study. *Phys. Rev. B* **1999**, *59*, 10583. (c) Goclon, J.; Grybos, R.; Witko, M.; Hafner, J. Relative Stability of Low-index V₂O₅ Surfaces: A Density Functional Investigation. *J. Phys.: Condens. Matter* **2009**, *21*, 095008. (d) Goclon, J.; Grybos, R.; Witko, M.; Hafner, J. Oxygen Vacancy Formation on Clean and Hydroxylated Low-index V₂O₅ Surfaces: A Density Functional Investigation. *Phys. Rev. B* **2009**, *79*, 075439.
- (34) (a) Smith, R. L.; Rohrer, G. S.; Lee, K. S.; Seo, D. K.; Whangbo, M. H. A Scanning Probe Microscopy Study of the (001) Surfaces of V₂O₅ and V₆O₁₃. *Surf. Sci.* **1996**, *367*, 87–95. (b) Costa, A. D.; Mathieu, C.; Barbaux, Y.; Poelman, H.; Dalmai-Vennik, G.; Fiermans, L. Observation of the V₂O₅ (001) Surface Using Ambient Atomic Force Microscopy. *Surf. Sci.* **1997**, *370*, 339–344.
- (35) Xiao, Z. R.; Guo, G. Y. Structural, Electronic and Magnetic Properties of V₂O_{5-x}: An ab Initio Study. *J. Chem. Phys.* **2009**, *130*, 214704.
- (36) Du, A. J.; Smith, S. C.; Yao, X. D.; Sun, C. H.; Li, L.; Lu, G. Q. The Role of V₂O₅ on the Dehydrogenation and Hydrogenation in Magnesium Hydride: An ab initio Study. *Appl. Phys. Lett.* **2008**, *82*, 163106.
- (37) (a) Liu, J.; Wang, X.; Peng, Q.; Li, Y. Vanadium Pentoxide Nanobelts: Highly Selective and Stable Ethanol Sensor Materials. *Adv. Mater.* **2005**, *17*, 764–767. (b) Li, G.; Pang, S.; Jiang, L.; Guo, Z.; Zhang, Z. Environmentally Friendly Chemical Route to Vanadium Oxide Single-Crystalline Nanobelts as a Cathode Material for Lithium-Ion Batteries. *J. Phys. Chem. B* **2006**, *110*, 9383–9386. (c) Chan, C. K.; Peng, H.; Twisten, R. D.; Jarausch, K.; Zhang, X. F.; Cui, Y. Fast, Completely Reversible Li Insertion in Vanadium Pentoxide Nanoribbons. *Nano Lett.* **2007**, *7*, 490–495.
- (38) Kresse, G. Efficient Iterative Schemes For ab Initio Total-energy Calculations Using a Plane-wave Basis Set. *Phys. Rev. B* **1996**, *S4*, 11169–11186.
- (39) Perdew, J. P.; Burke, K.; Ernzerhof, M. Generalized Gradient Approximation Made Simple. *Phys. Rev. Lett.* **1996**, *77*, 3865–3868.
- (40) Blöchl, P. E. Projector Augmented-wave Method. *Phys. Rev. B* **1994**, *50*, 17953–17979.
- (41) Grimme, S. Semiempirical GGA-Type Density Functional Constructed With a Long-Range Dispersion Correction. *J. Comput. Chem.* **2006**, *27*, 1787–1799.
- (42) Bučko, T.; Hafner, J.; Lebègue, S.; Ángyán, J. G. Improved Description of the Structure of Molecular and Layered Crystals: Ab Initio DFT Calculations with van der Waals Corrections. *J. Phys. Chem. A* **2010**, *114*, 11814–11824.
- (43) Botello-Méndez, A. R.; López-Urías, F.; Terrones, M.; Terrones, H. Magnetic Behavior in Zinc Oxide Zigzag Nanoribbons. *Nano Lett.* **2008**, *8*, 1562–1565.